Materials Science-Poland, 40(2), 2022, pp. 170-180
http://www.materialsscience.pwr.wroc.pl/
DOI: 10.2478/msp-2022-0019

Preparation of rGO/ZnO photoanodes and their DSSCs performance

Jiake Li[1,*], Lanxiang Wu[1], Wentao Li[1], Ying Chen[1], Xin Liu[1], Hedong Jiang[1], Pingchun Guo[1], Hua Zhu[2], Yanxiang Wang[1]

[1]School of Materials Science and Engineering, Jingdezhen Ceramic University, Jingdezhen City, China
[2]School of Mechanical and Electrical Engineering, Jingdezhen Ceramic University, Jingdezhen City, China

In this study, we report a mild and controllable preparation method for graphene oxide (GO) and ZnO ultrafine powder, respectively. On this basis, reduced graphene oxide (rGO)/ZnO composite powder for the photoanodes of dye-sensitized solar cells (DSSCs) was synthesized by chemical reduction method. Phase composition, microstructure, chemical structure, conductivity, and specific surface area were examined using X-ray diffraction (XRD), scanning electron microscopy (SEM), transmission electron microscopy (TEM), Fourier-transform infrared spectroscopy (FT-IR), Raman, and Brunauer-Emmett-Teller (BET) method, respectively. Photoelectric performance of DSSCs was studied by the current density-voltage (J-V), electrochemical impedance spectra (EIS) photoelectric test system. As rGO possesses higher adsorption capacity and excellent conductivity, hence it may effectively promote separation of electrons and holes, transmission ability of electrons and holes, and utilization of the light. By contrast, the as-synthesized zinc oxide (ZnO) may increase adsorption capacity of dye molecules, so photoelectric conversion efficiency (PCE) of the solar cells is increased by means of synergistic effects. When adding rGO in the rGO/ZnO composite powder at 1.25 wt%, PCE reaches to 6.27%, an increase of 20.6% more than that of pure ZnO as the photoanode.

Keywords: *improved Hummers method, GO, rGO/ZnO photoanodes, photoelectric performance*

1. Introduction

Graphene is formed by the close packing of monolayer carbon atoms with sp^2 orbital hybridization, and its crystal structure is a two-dimensional honeycomb-like structure. The unique two-dimensional structure endows graphene with high chemical stability, high specific surface area (theoretical value, 2.6×10^3 m^2/g), excellent conductivity (10^6 S/m), and high electron mobility (RT, room temperature, 1.5×10^4 $cm^2/(V{\cdot}s)$), as reported by Darabdhara et al. [1] and Zhu et al. [2]. Therefore, graphene may be applied in the field of dielectric materials according to Panahi-Sarmad et al. [3] and Bharatiya et al. [4], as a supercapacitor according to Kumar et al. [5] and Zhu et al. [6], and in photovoltaic devices according to Chang et al. [7] and Ubani et al. [8]. Dye-sensitized solar cells (DSSCs) are devices that transfer solar energy to electrical energy, and the photoanodes of DSSCs, which have a significant effect on efficiency of the cells, are usually made up of ZnO according to Cheng et al. [9], TiO_2 according to Ei-Ghamri et al. [10], and SnO_2 according to Zatirostami [11]. In the process of light absorption and electron generation of DSSCs, there are many defects (such as vacancies, impurities, and interface) in the interface between dyes and particles or between photoanodes and fluorine-doped tin oxide (FTO) glass, which reduces the generation and transmission of electrons and holes and increases the recombination, resulting in the reduction of photoelectric performance of DSSCs according to Babar et al. [12] and Dhamodharan et al. [13]. For example, Babar et al. [12] reported that TiO_2 with mesoporous structures have one of the best dye captivations, but the recombination rate is boosted by the perforation of the electrolyte into pores, so photoelectric conversion efficiency (PCE) of the cells is decreased. Therefore, application of graphene in the photoanodes can effectively increase efficiency of

* E-mail: jiakeli.jci@163.com

© Li et al. 2022. This is an open access article distributed under the Creative Commons Attribution-NonCommercial-NoDerivatives 4.0 License. (http://creativecommons.org/licenses/by-nc-nd/4.0/)

separation and transmission of electrons and holes, so as to improve the photoelectric performance of DSSCs according to Sarkar et al. [14] and Patil et al. [15]. For example, Sarkar et al. [14] reported the synthesis of nickel sulfide (NiS) nanoparticles decorated reduced graphene oxide (rGO) as counter electrode (CE) in DSSC. The charge transfer resistance (R_{ct}) of the cell was decreased from 3 Ω/cm^2 to 1.5 Ω/cm^2, so PCE was increase from 7.7% to 9.5%.

In general, graphene oxide (GO) was prepared by the traditional Hummers method with the reactive system temperature, which is controlled from low to high temperature, as reported by Zhu et al. [2] and Yoo and Park [16]. Due to the layered structure of graphite, it is enlarged in the late stage of oxidation, so the high-temperature environment makes reaction violent and difficult to control. Moreover, the traditional Hummers method for preparing GO also has other disadvantages, such as environmental pollution, and other defects in GO due to insufficient oxidation, as reported by Aixart et al. [17] and Hou et al. [18]. Therefore, it is of great significance to explore a mild and easily controlled process to prepare high-quality GO.

In addition, there are many kinds of methods for preparation of ultrafine powder for photoanodes, such as the sol–gel method according to Balachandran et al. [19], hydrothermal method according to Jiao and Jiao [20], coprecipitation method according to Wang et al. [21], and combustion method according to Liu et al. [22]. Among the above preparation technologies, solution combustion method is a new method for synthesis of ultrafine powder, which possesses advantages such as low synthesized temperature, simple process conditions, easy-control process of preparation, short reaction time, and the synthesized powder with small and uniform particle size, as reported by Striker and Ruud [23] and Boobalan et al. [24]. For example, Boobalan et al. [24] reported that ZrO_2 powder was prepared by the combustion method using sucrose as fuel and zirconyl nitrate as oxidant in aqueous solution, and oxidant to fuel molar ratio was optimized (0.2) to prepare nanocrystalline ZrO_2 with particle size of 5–30 nm.

In this study, GO was prepared by the improved Hummers method with the reactive system temperature from high, low to medium, and this preparation process was mild and easy to control. In addition, ZnO ultrafine powder was synthesized by solution combustion method. On this basis, rGO/ZnO composite powder, which was used to prepare the photoanodes of solar cell, was synthesized by chemical reduction method. Phase composition, microstructure, and PCE of the synthesized powder and the solar cells were examined using XRD, SEM, TEM, FT-IR, Raman, BET and photoelectric conversion test system.

2. Experiment

2.1. Materials

Microcrystalline graphite (average particle size 30 μm, concentration >98%), concentrated sulfuric acid (H_2SO_4, concentration 96%–98%), concentrated hydrochloric acid (HCl, concentration 36%), hydrogen peroxide (H_2O_2, concentration 30%), potassium permanganate ($KMnO_4$), potassium persulfate ($K_2S_2O_8$), phosphorus pentoxide (P_2O_5), zinc nitrate hexahydrate ($(Zn(NO_3)_2{\cdot}6H_2O$), sucrose ($C_{12}H_{22}O_{11}$), zinc acetate ($Zn(Ac)_2{\cdot}2H_2O$), polyethylene glycol-300 (PEG-300), hydrazine hydrate (H_6N_2O, 80%), ethyl cellulose (viscosity:10 cp), ethyl cellulose (viscosity:46 cp), and terpineol and anhydrous ethanol (C_2H_6O) were used. All reagents were of analytical grade and used without further purification.

2.2. Synthesis of GO

GO was prepared by the improved Hummers method with the reactive system temperature from high, low to medium, and the schematic diagram of GO preparation process is as shown in Figure 1.

In the high-temperature oxidation period, 9.7 mL H_2SO_4 was added into a 500 mL beaker accurately, and 1.2 g microcrystalline graphite, 2 g $K_2S_2O_8$, and 1.2 g P_2O_5 were successively added to a beaker under stirring condition. Then the beaker was placed in a water bath at 80°C with stirring for 4.5 h. In the low-temperature oxidation period, 50 mL H_2SO_4 and 6 g $KMnO_4$ were added

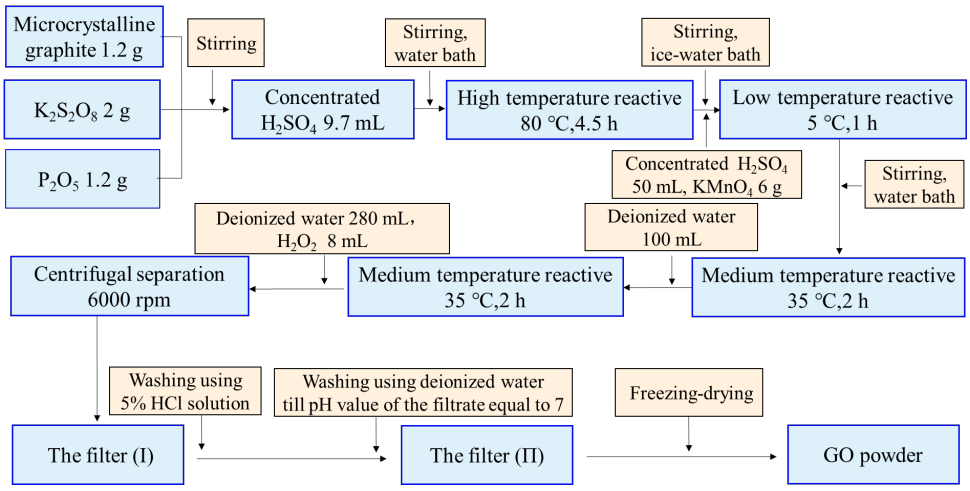


Fig. 1. The schematic diagram of GO preparation process. GO, graphene oxide

to the above mixed suspension in an ice-water bath at 5°C with stirring for 1 h, and a dark green suspension was obtained. In the medium temperature oxidation period, the water bath temperature was raised to 35°C, and the dark green suspension was stirred for 2 h, and then 100 mL deionized water was added to the suspension with stirring for 2 h. Finally, 280 mL deionized water was added to the above suspension with stirring condition, and then 8 mL H_2O_2 was added until the suspension turned to bright yellow. The bright yellow suspension was filtered and washed using 5% HCl solution and deionized water several times until the pH value of the filtrate was equal to 7. GO powder was obtained by freeze-drying the filter. The freeze-drying process consists of two stages. The first stage is that of pre-freezing, where the temperature, time, and vacuum degree were – 40°C, 5 h, and 1.013×10^5 Pa, respectively; the second stage was the drying which is from – 40°C to 5°C with heating rate of 0.05°C/min under vacuum degree of 30 Pa.

2.3. Synthesis of ZnO Ultrafine Powder

ZnO ultrafine powder was synthesized by the solution combustion method. The precursor solution was obtained by mixing zinc nitrate, sucrose, and deionized water with a certain proportion. According to the principle of propellant chemistry, sucrose-zinc nitrate solution was completely combusted with releasing of N_2, CO_2, and H_2O gas according to Striker and Ruud [23], and the combustion reaction equation was as follows:

$$\mathrm{Zn(NO_3)_2} + \frac{5\varphi}{24}\mathrm{C_{12}H_{22}O_{11}} + \frac{5(\varphi-1)}{2}\mathrm{O_2} \xrightarrow{\text{igniting}} \mathrm{ZnO} + \frac{55\varphi}{24}\mathrm{H_2O} + \frac{5\varphi}{2}\mathrm{CO_2} + \mathrm{N_2} \quad (1)$$

where φ is the molar ratio of sucrose and nitrate, which is called stoichiometric coefficient. When φ is equal to 1, the system is completely combusted according to the theory. Considering the factors such as heat dissipation of the system, φ equal to 1.5 was chosen (excessive fuel). Raw materials were weighed according to stoichiometric ratio (see Eq. (1)) and dissolved in deionized water. In the precursor solution, Zn^{2+} concentration was 0.2 mol/L and sucrose concentration was determined by using Eq. (1). A certain volume of precursor solution was taken to a refractory crucible and then placed in a furnace at 500°C. Subsequently, combustion reaction was occurred and powder was obtained after completion of the reaction. The detailed preparation process is shown in the relevant literature according to Li and Liu [25].

2.4. Synthesis of rGO/ZnO Composite Powder

GO powder was accurately weighed and dispersed in 100 mL deionized water to prepare

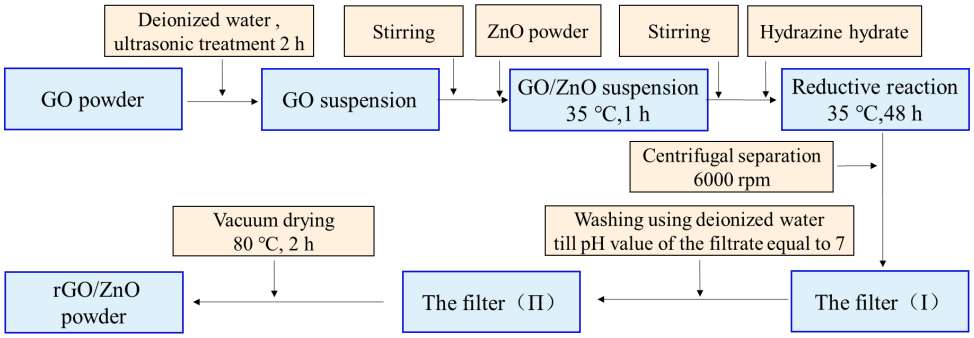


Fig. 2. Schematic diagram of the rGO/ZnO composite powder preparation process. GO, graphene oxide; rGO, reduced graphene oxide

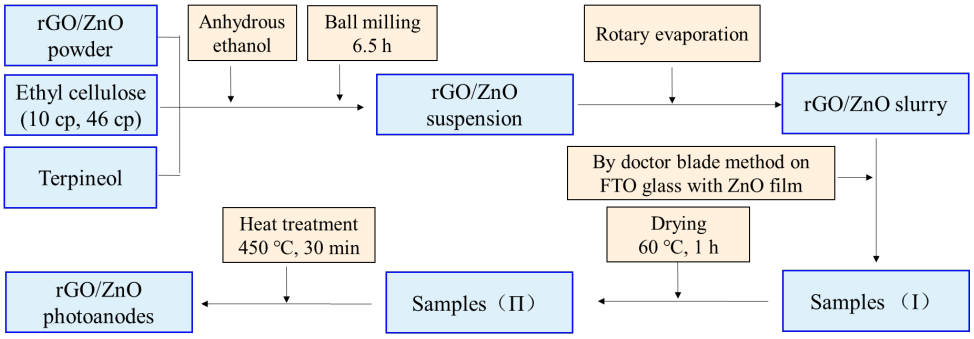


Fig. 3. Schematic diagram of the rGO/ZnO photoanodes preparation process. GO, graphene oxide; rGO, reduced graphene oxide

GO suspension at concentrations of 3.3 mg/mL, 9.8 mg/mL, 16.3 mg/mL, 22.8 mg/mL, and 29.3 mg/mL, respectively. After strong ultrasonic treatment for 2 h, the stable GO suspension was obtained. Then, the above GO suspension (1 mL) and ZnO powder (1.3 g) were mixed, respectively, with stirring for 60 min in a water bath at 35°C, and then 30 μL 80% hydrazine hydrate was added and stirred for 48 h to reduce it. Finally, the mixed suspension of rGO and ZnO was filtered and centrifuged several times until the pH value of the filtrate was equal to 7. Then the filter was dried in vacuum at 80°C for 2 h, so rGO/ZnO composite powder with 0%, 0.25%, 0.75%, 1.25%, 1.75%, and 2.25% rGO were obtained, respectively. The schematic diagram of rGO/ZnO composite powder preparation process is shown in Figure 2.

2.5. Preparation of DSSCs

2.5.1. Preparation of rGO/ZnO photoanodes

For the preparation of ZnO film, precursor sol (0.2 mol/mL) was prepared by a water bath with zinc acetate, ammonia water, polyethylene glycol, and anhydrous alcohol as raw materials, and then precursor sol was coated on FTO glass by the spin coating method. Subsequently, ZnO film was obtained by further heat treatment at 500°C for 30 min.

In the preparation of rGO/ZnO photoanodes, a slurry was prepared by ball milling and rotary evaporation using rGO/ZnO composite powder, ethyl cellulose (viscosity: 10 cp), ethyl cellulose (viscosity: 46 cp), and terpineol as raw materials with mass ratio of 1:0.22:0.28:4.05, and an appropriate amount of anhydrous ethanol was added as solvent. The slurry was coated by doctor blade method on the FTO glass with ZnO film, and finally rGO/ZnO

photoanodes were obtained by drying at 60°C for 60 min and heat treatment at 450°C for 30 min. The schematic diagram of rGO/ZnO photoanodes preparation process is shown in Figure 3.

2.5.2. Assembly of DSSCs

rGO/ZnO photoanodes were immersed into N719 dye solution for dark sensitization for 2 h, and then an appropriate amount of liquid electrolyte was dropped between the photoanodes and Pt CE. Finally, DSSCs with "sandwich" structure were assembled using swallowtail clamp.

The solar cells assembled with the photoanodes, which contained rGO with 0%, 0.25%, 0.75%, 1.25%, 1.75%, and 2.25%, were numbered as D0, D1, D2, D3, D4, and D5, respectively.

2.6. Materials Characterization

Phase composition of the samples was analyzed by using XRD (D8-Advance, Brucker, Karlsruhe, Germany) with CuKα radiation (λ = 0.15418 nm) and step scan mode (range: 5°–90° of 2θ, step-time: 0.60 s, and step-size: 0.04°). The microstructure of the samples was characterized by using SEM (JSM-6700F, JEOL, Tokyo, Japan) and TEM (JEM-2010 HR, JEOL,Tokyo, Japan). Chemical structure of the samples was detected by using FT-IR (Nicolet 5700, Massachusetts , America) between 400/cm and 4,000/cm wavenumber with a resolution of 4/cm and Raman spectrometer (in Via, Renishaw, Gloucestershire, England) between 100/cm and 3,200/cm wavenumber with a resolution of 1/cm. The specific surface area of the samples was tested by using automatic physical-chemical adsorption instrument (ASAP-2020, Micromeritics, America) with high-purity nitrogen as adsorbent, and it was calculated by using BET (Brunauer-Emmett-Teller) method. Conductivity of rGO was tested by using a digital four-point probe tester (ST-2258A, Jingle, Suzhou, China). Photoelectric conversion performance of the solar cells was tested by using solar simulated light source (SXDN-150, Nowdata Corporation, Tokyo, Japan) with light intensity of AM1.5 (100 mW/cm^2) and the area of the solar cells was 0.16 cm^2. The outer quantum efficiency of the solar cells was tested by using a photon-electron conversion tester (Solar Cell Scan100, ZOLIX, Beijing, China), and testing wavelength range was from 300 nm to 800 nm. EIS of the solar cells was tested by using electrochemical workstation (Zahner Zennium, Kronach, Germany) with detection frequency range from 10^{-1} Hz to 10^5 Hz.

3. Results and Discussion

3.1. Phase Analysis

Figure 4 shows XRD patterns of the samples prepared by the improved Hummers method. It can be seen from Figure 4 that there was an obvious characteristic diffraction peak at 2θ = 10°, which is consistent with the characteristic diffraction peak of GO according to Zhu et al. [2], indicating that GO is successfully prepared by the improved Hummers method.

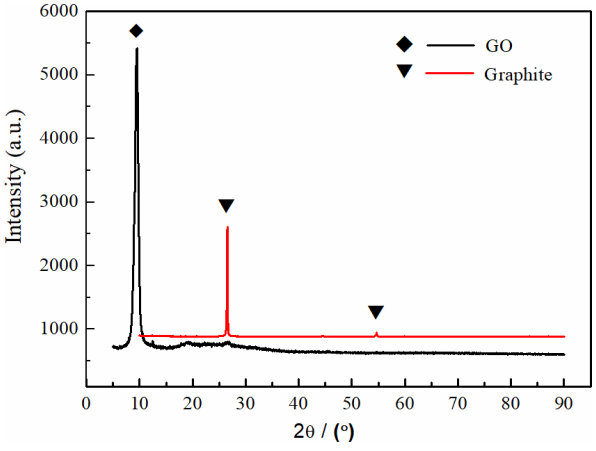


Fig. 4. XRD patterns of the samples prepared by the improved Hummers method. GO, graphene oxide

According to Bragg equation 2dsinθ = nλ, the interlaminar spacing for GO, rGO, and graphite is 0.81 nm, 0.41 nm, and 0.34 nm, respectively. The increase of the interlaminar spacing of GO is due to the insertion of a large number of oxygen-containing functional groups into carbon layer during oxidation process (see "3.2 Infrared and Raman Spectra Analysis" section, and with regard to rGO, due to the loss of the functional groups (see "3.2 Infrared and Raman Spectra Analysis" section), the interlayer spacing decreases, but it is still greater than that of graphite. In addition, the characteristic

diffraction peaks of GO tended to widen comparing with the characteristic diffraction peaks of graphite. This is due to covalent bonding between functional groups and carbon atoms, resulting in the bending and folding of GO microstructure (as shown in Figure 4), and causing order degree of GO lamellar is lowered in the vertical direction than that of graphite as reported by Zhu et al. [2].

Figure 5(A) shows XRD pattern of the sample prepared by solution combustion method. It can be seen from Figure 5(A) that these typically peaks can be indexed to the crystal planes (100), (002), (101), (102), (110), (103), (112), and (201) (JCPDS cards No: 36-1451, ZnO), respectively. And there are no other impurity peaks in the pattern, indicating that the as-synthesized ZnO has high purity. Besides, it can also be seen from the characteristic peaks that the as-synthesized ZnO possesses hexagonal structure.

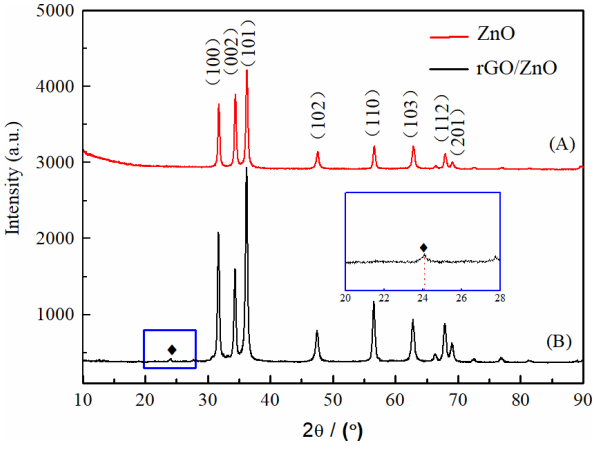


Fig. 5. XRD patterns **(A)** ZnO prepared by solution combustion method, **(B)** rGO/ZnO with 1.25% rGO prepared by the chemical reduction method. rGO, reduced graphene oxide

Moreover, Figure 5(B) shows XRD pattern of the composite powder prepared by the chemical reduction method. It may also be seen from the pattern that there is a characteristic diffraction peak of rGO at $2\theta = 24^\circ$ according to Park et al. [26], and this indicates that GO is reduced to rGO. Through XRD analysis of the composite powder, it indicates that rGO/ZnO composite powder is synthesized.

3.2. Infrared and Raman Spectra Analysis

Figure 6 shows FT-IR spectra of GO and rGO/ZnO prepared by the improved Hummers and the chemical reduction method, respectively. It can be seen from FT-IR spectrum of GO that there are many characteristic peaks of oxygen-containing functional groups between GO layers, among which absorption peak near 3,420/cm is caused by stretching vibration of -OH group; an obvious absorption peak can be found near 1,730/cm, which is main deformation peak caused by stretching vibration of –COOH and C=O groups at the edge of GO layer; peak near 1,625/cm corresponds to bending vibration of –OH group adsorbed on water molecule, while absorption peak near 1,220/cm is caused by stretching vibration of C–O. Due to oxygen-containing functional groups such as –OH, –COOH, C=O, and C–O, they can enter into graphite interlayer during oxidation reaction, and then destroyed the crystal structure of graphite. As a result, the layered structure of graphite was transformed into a separated lamellar structure, so GO is formed as reported by Shuai et al. [27] and Zaaba et al. [28]. Moreover, it can be seen from FT-IR spectrum of rGO/ZnO that absorption peak of –OH groups disappear, and absorption peaks of -COOH, C=O, and C–O disappear or decrease, and stretching vibration peak of C=C (1,564/cm) appears. In addition, there are many absorption peaks near 500/cm, which can be attributed to the vibrational absorption of Zn–O bond in ZnO. These indicate rGO/ZnO composite powder is synthesized by the chemical reduction method. Moreover, other rGO/ZnO with different contents of rGO have similar FT-IR spectra.

Raman spectra for GO and rGO are shown in Figure 7. The observed peaks near 1,350/cm and 1,590/cm can be assigned to D (κ-point phonons breathing mode) and G (carbon atoms sp^2 bonds) bands, respectively. The ratio of the integral area values of D and G peaks (I_D/I_G, i.e., degree of disorder) changes from 1.05 for GO to 1.11 for rGO, which indicates an increase of defective sites by the chemical reduction and conversion of GO to rGO. However, there are still relatively low level of defects in rGO.

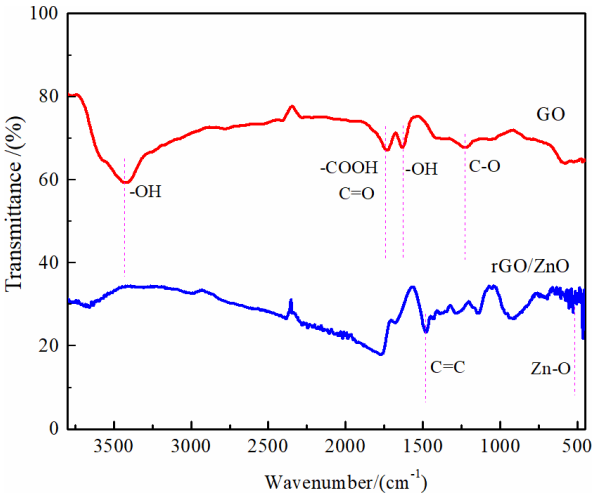


Fig. 6. FT-IR spectra of GO prepared the improved Hummers, and rGO/ZnO with 1.25% rGO prepared by chemical reduction method. GO, graphene oxide; rGO, reduced graphene oxide

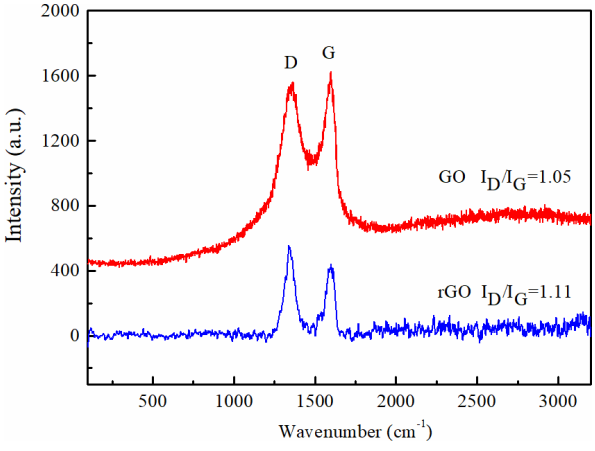


Fig. 7. Raman spectra of GO and rGO prepared by the improved Hummers and the chemical reduction methods, respectively. GO, graphene oxide; rGO, reduced graphene oxide

3.3. Microstructure Analysis

SEM images of GO are shown in Figure 8. It can be seen from Figure 8A that GO has a layered structure, and there are a lot of folds on the surface of the layers, so the as-synthesized GO has a higher specific surface area of 650 m^2/g. These indicate that GO has lost surface characteristics of graphite and changed from a flat and smooth surface to a rough and stepped surface. Moreover, it may be further seen from Figure 8(B) that there are different distances between GO layers. This is due to the strong oxidation of oxidant, hydroxyl, carbonyl, and other groups are introduced to the edge and interlayer of GO. At the same time, surface energy of the layers is increased when graphite is oxidized to GO. To maintain the stability of the layered surface, a large number of folds are formed on the surface. These indicate that the as-prepared GO has good microstructure.

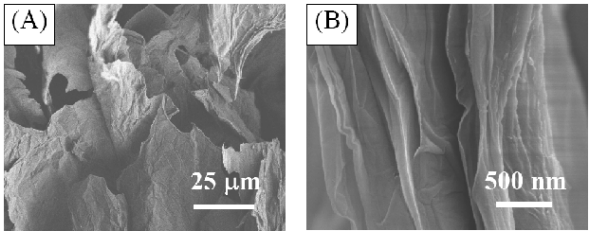


Fig. 8. SEM images of GO prepared by the improved Hummers method: **(A)** low-magnification and **(B)** high-magnification. GO, graphene oxide

Figure 9 shows TEM images and selected area electron diffraction (SAED) of GO. It can be seen from Figure 9A that the layered GO is stacked disorderly and has good light transmittance near the edge. Figure 9B shows that GO presents transparent characteristics. To decrease the surface energy, the layered surface of GO is uneven and there are a lot of folds, which is consistent with the SEM analysis results. In addition, it can be seen from the inset in Figure 9B that there is a series of halo around the bright spot, which indicates that the as-synthesized GO has a polycrystalline structure.

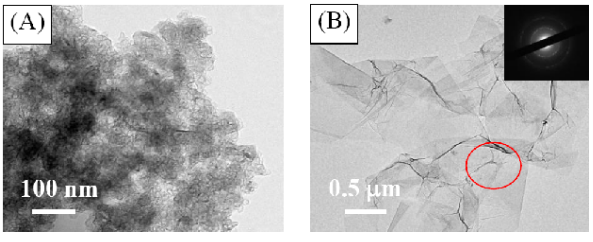


Fig. 9. TEM images **(A)** and its SAED of GO **(B)** prepared by the improved Hummers method. GO, graphene oxide

Figure 10 shows SEM images of ZnO powder, rGO, and the cross section of rGO/ZnO pho-

toanode. Figure 10A shows that the as-synthesized ZnO shows short rods with particle size about 50 nm, and has good dispersibility, while Figure 10B shows that rGO has a typical layered structure, and the layered structure has a little agglomerate than that of GO. The rGO/ZnO photoanode shows porous and high porosity (see Figure 10C), and it can also be seen from Figure 10D that rGO/ZnO porous layer consists of rod and flake particles. The short rod particles is ZnO while the lamellar with size about 100–200 nm is rGO. In addition, it can be further seen from Figure 10D that ZnO film is about 200 nm between rGO/ZnO layer and FTO glass, which may increase utilization of incident light, and binding ability between rGO/ZnO layer and FTO glass. The photoanode with porous structure is beneficial to increasing adsorption capacity of dye molecules. Moreover, other photoanodes with adding different contents of rGO have similar microstructure.

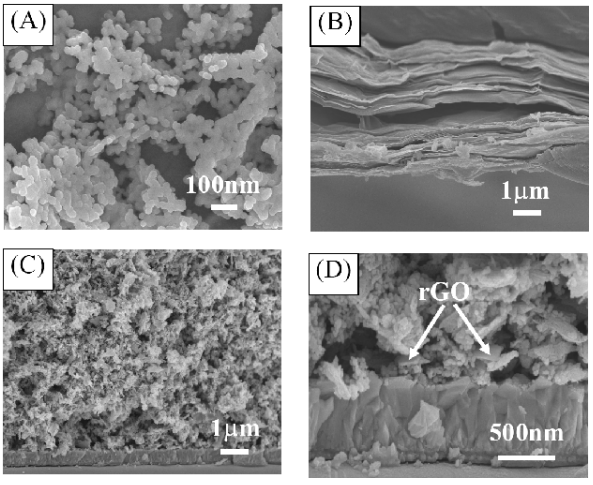


Fig. 10. **(A)** SEM images of the as-synthesized ZnO by solution combustion, **(B)** rGO, **(C)** the cross section of rGO/ZnO photoanode at low-magnification, and **(D)** high-magnification. *Note*: rGO adding content 1.25%. rGO, reduced graphene oxide

3.4. Photoelectric Performance Analysis of DSSCs

The J-V curves of the assembled solar cells with rGO/ZnO photoanodes are shown in Figure 11, and photoelectric performance parameters of the corresponding solar cells are shown in Table 1. It can be seen from Figure 11 and Table 1 that the effects of the photoanodes by adding different contents of rGO on the performance of the solar cells are very remarkable. PCE of D0 assembled by the photoanode without rGO (the pure ZnO) is 5.20%, and J_{sc}, V_{oc}, and FF are 0.63V, 12.73 mA/cm^2, and 64.70%, respectively. By increasing the content of adding rGO in the photoanodes, PCE, J_{sc}, and FF values of DSSCs increase initially and then decrease. The V_{oc} of the corresponding solar cells are maintained between 0.63 V and 0.66 V. When adding content of rGO in the photoanode at 1.25%, PCE of D3 reaches the maximum value of 6.27%, and J_{sc}, V_{oc}, and FF are 0.66 V, 13.11 mA/cm^2, and 72.71%, respectively. With the further increase of rGO content in the photoanodes, PCE of the solar cells decreases gradually. For example, when adding content of rGO in the photoanodes is 2.25%, PCE of D5 is decreased to 5.10%.

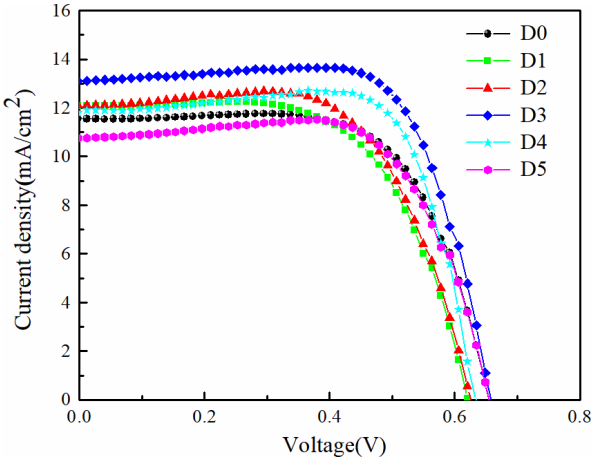


Fig. 11. J-V curves of DSSCs assembled by rGO/ZnO as the photoanodes by adding different contents of rGO. DSSCs, dye-sensitized solar cells; rGO, reduced graphene oxide

The reasons for the above experimental results can be explained as follows: With pure ZnO as the photoanode, the solar cell has a relatively high efficiency (5.20%). This is because ZnO has a small crystal size (50 nm), relatively larger specific surface area (24.83 m^2/g), and perfect crystal structure, but the slow separation rate of electrons and

holes, and low transmission rate of electrons from ZnO conduction band to FTO glass lead to very easy recombination of electrons and holes, and thus PCE of the solar cell is lower than that of theoretical value as reported by Babar et al. [12] and Dhamodharan et al. [13]. As the as-synthesized rGO has excellent conductivity (5,530 S/m) and larger specific surface area (450 m^2/g), when rGO is added to the photoanodes, it promotes separation of electrons and holes, decreases their recombination as reported by Wu et al. [29], and increases adsorption capacity of dye molecules (see Figure 10C), so PCE of the solar cells is increased. However, when adding content of rGO is too much, the content of ZnO in the photoanodes is relatively reduced. Subsequently, the number of electrons and holes is reduced, which is excited by photoelectric effect, and then PCE of the solar cells are lowered.

Table 1. Performance parameters of DSSCs assembled by rGO/ZnO as the photoanodes by adding different contents of rGO

Samples	Adding content /wt.%	V_{oc} /V	J_{sc} /mA /cm^2	FF/%	PCE /%
D0	0	0.63	12.73	64.70	5.20
D1	0.25	0.63	12.76	66.82	5.27
D2	0.75	0.65	12.83	66.94	5.42
D3	1.25	0.66	13.11	72.71	6.27
D4	1.75	0.63	11.79	69.92	5.51
D5	2.25	0.65	10.83	69.60	5.10

DSSCs, dye-sensitized solar cells; PCE, photoelectric conversion efficiency; rGO, reduced graphene oxide.

Figure 12 shows the external quantum efficiency (EQE) of D0, D1, D2, D3, D4, and D5. Figure 12 shows that with the increase of rGO content in the photoanodes, the EQE of the solar cells have a prominent enhancement trend in 400—700 nm. When adding content of rGO in the photoanodes is 1.25%, D3 has a maximum value of EQE. With further increase of rGO content in the photoanodes, the EQE of the solar cells decreases gradually. This is due to rGO that can improve the absorption ability and utilization efficiency of DSSCs for the light, which increases the number of photogenerated electrons and electrons mobility as reported by Riaza et al. [30] and Kumar et al. [31], so PCE of the solar cells is increased.

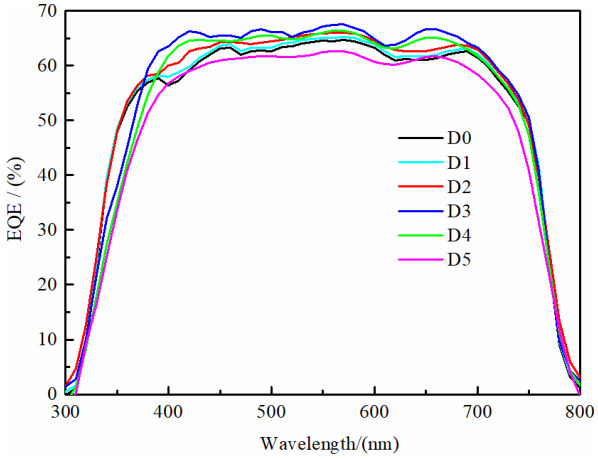


Fig. 12. EQE curves of D0, D1, D2, D3, D4, and D5. EQE, external quantum efficiency

Figure 13 shows Nyquist curves of D0, D1, D2, D3, D4, and D5 under dark conditions. Figure 13 shows that there are two arcs in the high-frequency region and the low-frequency region, in which the high-frequency region represents the charge transfer resistance (R_{ct}) at the interface between the photoanodes and FTO glass, and the low-frequency region represents the composite resistance (R_{rec}) at the interface of the photoanodes-dye-electrolyte. In the high-frequency region, the charge transfer resistance R_{ct} of D3 is lower than those of the other solar cells, while in the low-frequency region, the composite resistance R_{rec} of D3 is higher than those of the other solar cells, so D3 has the highest PEC. These results indicate that an appropriate amount of rGO added to the photoanodes can promote the transport of electrons and holes between the photoanodes and FTO glass, and reduces recombination of electrons and holes at the interface of the photoanodes-dye-electrolyte according to Omar et al. [32] and Quang et al. [33], and thus improves the performance of the solar cells. This also confirms that rGO may increase PCE of the solar cells from the electrochemical point of view.

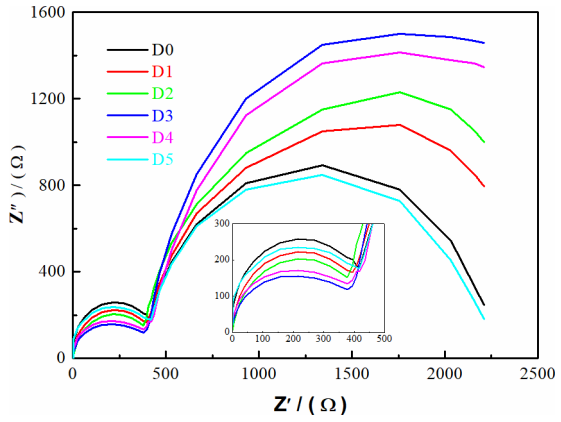


Fig. 13. Nyquist curves of D0, D1, D2, D3, D4, and D5 under dark conditions

4. Conclusions

GO is prepared by the improved Hummers method with the reactive system temperature from high, low to medium, and the whole reaction process is very mild and controllable. Oxygen-containing function groups, such as carboxyl, hydroxyl, and carbonyl groups, are attached between the layers and the edges. The interlayer space and specific surface area of GO are 0.81 nm and 650 m^2/g, respectively; and specific surface area and conductivity of rGO are 450 m^2/g and 5,530 S/m, respectively. For the as-synthesized ZnO, specific surface area and particle size are 24.83 m^2/g and 50 nm, respectively.

rGO/ZnO composite powders are synthesized by chemical reduction method, and the photoanodes are prepared with rGO/ZnO composite powder. As rGO has higher adsorption capacity and excellent conductivity, it may effectively promote separation of electrons and holes, transmission ability of electrons and holes, and utilization of the light, while the as-synthesized ZnO may increase adsorption capacity of dye molecules, so PCE of the solar cells is increased by means of synergistic effects. When adding content of rGO at 1.25%, D3 has an optimum photoelectric conversion performance, and PCE, V_{oc}, J_{sc}, and FF are 6.27%, 0.66 V, 13.11 mA/cm^2, and 72.71%, respectively. PCE of D3 is increased by 20.6% higher than that of DSSCs assembled with pure ZnO as the photoanode.

Declaration of Competing Interests

The authors declare that they have no known competing financial interests or personal relationships that could have appeared to influence the work reported in this paper.

Acknowledgements

This work was supported by the Science and Technology Research Project of Jiangxi Provincial Education Department of China (No. GJJ201315, GJJ201316, and GJJ190693) and National Natural Science Regional Fund, China (No. 61764007).

References

[1] Darabdhara G, Das MR, Singh SP, Rengan AK, Boukerroub R. Ag and Au nanoparticles/reduced graphene oxide composite materials: synthesis and application in diagnostics and therapeutics. Adv Colloid Interface. 2019;271:101991.

[2] Zhu YW, Murali S, Cai WW, Li XS, Ji WS, Jeffrey RP, et al. Graphene and graphene oxide: synthesis, properties, and applications. Adv Mater. 2010;22(35):3906–24.

[3] Panahi-Sarmad M, Zahiri B, Noroozi M. Graphene-based composite for dielectric elastomer actuator: a comprehensive review. Sensor Actuat A Phys. 2019;293:222–41.

[4] Bharatiya D, Parhi B, Swain SK. Preparation, characterization and dielectric properties of GO based ZnO embedded mixed metal oxides ternary nanostructured composites. J Alloys Compd. 2021;869:159274.

[5] Kumar R, Kim HJ, Park S, Srivastava A, Oh IK. Graphene-wrapped and cobalt oxide-intercalated hybrid for extremely durable supercapacitor with ultrahigh energy and power densities. Carbon. 2014;79:192–202.

[6] Zhu YC, Jiang HD, Ye XK, Yue ZY, Wang LH, Jia CY. Similar "relay race" capacitance behaviors of folded graphene films based high-performance supercapacitors. J Power Sources. 2020;460:228108.

[7] Chang DW, Choi HJ, Filer A, Baek JB. Graphene in photovoltaic applications: organic photovoltaic cells (OPVs) and dye-sensitized solar cells (DSSCs). J Mater Chem A. 2014;2(31):12136–50.

[8] Ubani CA, Ibrahim MA, Teridi MAM, Sopian K, Ali J, Chaudhary KT. Application of graphene in dye and quantum dots sensitized solar cell. Sol Energy. 2016;137:531–50.

[9] Cheng HY, Wang YX, Guo PC, Yang ZS. High-efficiency dye-sensitized solar cells based on a ZnO nanorod/nanosheet hierarchical structure. Energy Technol. 2018;6:1161–7.

[10] Ei-Ghamri HS, El-Agez TM, Taya SA, Abdel-Latif MS, Batniji AY. Dye-sensitized solar cells with natural dyes extracted from plant seeds. Mater Sci Poland. 2014;32(4):547–54.

[11] Zatirostami A. SnO_2-based DSSC with SnSe counter electrode prepared by sputtering and selenization of Sn: effect of selenization temperature. Mat Sci Semicon

Proc. 2021;135:106044.
[12] Babar F, Mehmood U, Asghar H, Mehdi MH, Khan AUH, Khalid H, et al. Nanostructured photoanode materials and their deposition methods for efficient and economical third generation dye-sensitized solar cells: a comprehensive review. Renew Sust Energ Rev. 2020;129:109919.
[13] Dhamodharan P, Chen J, Manoharan C. Fabrication of in doped ZnO thin films by spray pyrolysis as photoanode in DSSCs. Surf Interfaces. 2021;23:100965.
[14] Sarkar A, Chakraborty AK, Bera S. NiS/rGO nanohybrid: an excellent counter electrode for dye sensitized solar cell. Sol Energ Mat Sol C. 2018;182:314–20.
[15] Patil JV, Mali SS, Patil AP, Patil PS, Hong CK. Highly efficient mixed-halide mixed-cation perovskite solar cells based on rGO-TiO_2 composite nanofibers. Energy. 2019;189:116396.
[16] Yoo MJ, Park HB. Effect of hydrogen peroxide on properties of graphene oxide in Hummers method. Carbon. 2019;141:515–22.
[17] Aixart J, Díaz F, Llorca J, Rosell-Llompart J. Increasing reaction time in Hummers' method towards well exfoliated graphene oxide of low oxidation degree. Ceram Int. 2021;47(8):22130–7.
[18] Hou YG, Lv SH, Liu LP, Liu X. High-quality preparation of graphene oxide via the Hummers' method: understanding the roles of the intercalator, oxidant, and graphite particle size. Ceram Int. 2020;46(8):2392–402.
[19] Balachandran K, Kalaivani T, Thangaraju D, Mageswari S, Preethi A. Fabrication of photoanodes using sol-gel synthesized Ag-doped TiO_2 for enhanced DSSC efficiency. Mater Today. 2021;32:515–21.
[20] Jiao CR, Jiao J. Properties of ytterbium silicate powder for environmental barrier coating with hydrothermal method. Journal of Ceram. 2021;42(3):445–51 (in Chinese).
[21] Wang Y, Luo F, Ling Z, Zhu D, Zhou W. Microwave dielectric properties of Al-doped ZnO powders synthesized by coprecipitation method. Ceram Int. 2013;39(8):8723–7.
[22] Liu F, Huang JG, Jiang JH. Synthesis and characterization of red pigment $YAl_{1-y}Cr_yO_3$ prepared by the low temperature combustion method. J Eur Ceram Soc. 2013;33(13–14):2723–9.
[23] Striker T, Ruud JA. Effect of fuel choice on the aqueous combustion synthesis of lanthanum ferrite and lanthanum manganite. J Am Ceram Soc. 2010;93(9):2622–9.
[24] Boobalan K, Vijayaraghavan R, Chidambaram K, Mudali UMK, Raj B. Preparation and characterization of nanocrystalline zirconia powders by the glowing combustion method. J Am Ceram Soc. 2010;93:3651–6.
[25] Li JK, Liu X. Effect of fuel on morphology and photocatalytic performance of ZnO nanorods synthesized by solution combustion method. J Inorg Mater. 2013;28(8):880–4 (in Chinese).
[26] Park S, An J, Potts JR, Velamakanni A, Murali S, Ruoff RS. Hydrazine-reduction of graphite- and graphene oxide. Carbon. 2011;49(9):3019–23.
[27] Shuai SR, Liu Y, Zhao C, Zhu HY, Li Y, Zhou KH, et al. Improved synthesis of graphene oxide with controlled oxidation degree by using different dihydrogen phosphate as intercalators. Chem Phys. 2020;539:110938.
[28] Zaaba NI, Foo KL, Hashim U, Tan SJ, Liu WW, Voon CH. Synthesis of graphene oxide using modified hummers method: solvent influence. Procedia Eng. 2017;184:469–77.
[29] Wu J, Li LY, Li XA, Min X, Xing Y. A novel 2D graphene oxide modified α-$AgVO_3$ nanorods: design, fabrication, and enhanced visible-light photocatalytic performance. J Adv Ceram. 2022;11:308–20.
[30] Riaza R, Alia M, Maiyalaganc T, Anjuma AS, Lee S, Ko MJ, et al. Dye-sensitized solar cell (DSSC) coated with energy down shift layer of nitrogen-doped carbon quantum dots (N-CQDs) for enhanced current density and stability. Appl Surf Sci. 2019;483:425–31.
[31] Kumar V, Gupta R, Bansal A. Role of chenodeoxycholic acid as co-additive in improving the efficiency of DSSCs. Sol Energy. 2020;196:589–96.
[32] Omar A, Ali MS, Rahim NA. Electron transport properties analysis of titanium dioxide dye-sensitized solar cells (TiO_2-DSSCs) based natural dyes using electrochemical impedance spectroscopy concept: a review. Sol Energy. 2020;207:1088–121.
[33] Quang LND, Kaliamurthy AK, Hao NH. Co-sensitization of metal based N719 and metal free D35 dyes: an effective strategy to improve the performance of DSSC. Opt Mater. 2021;111:110589.

Received 2021-08-21
Accepted 2022-06-13